SAND97-1186C
CONF-9709107--

# Strength and tribology of bulk and electroformed nickel amorphized by implantation of titanium and carbon

S. M. Myers, J. A. Knapp, D. M. Follstaedt, M. T. Dugger, and T. R. Christenson

Sandia National Laboratories, Albuquerque, NM 87185-1056

## Abstract

Dual ion implantation of titanium and carbon was shown to produce an amorphous layer of exceptional strength within annealed bulk Ni and electroformed Ni and $Ni_{80}Fe_{20}$ materials used in micro-electromechanical systems. The intrinsic elastic and plastic mechanical properties of the implanted region were quantified using nanoindentation testing in conjunction with finite-element modeling, and the results were interpreted in the light of microstructures observed by electron microscopy. The implantation treatment was found to produce substantial reductions in unlubricated friction and wear.



## DISCLAIMER

## Introduction

Dual ion implantation of Ti and C, or Ti implantation with C incorporation from the surface, was previously found to produce an amorphous layer in Fe [1,2], Ni [3], and a range of steels [4-6]. This treatment improved the tribological properties of steels during unlubricated sliding contact of a hard steel pin on a treated disc, with friction typically being reduced by half and wear rate by an order of magnitude [4,7-10]. Additionally, nanoindentation testing indicated that a high-strength bearing steel was further hardened by implanting both Ti and C [11]. Amorphizations of Ni by implantation of B or P, or by cryogenic-temperature implantation of C, reduced friction and wear during testing with a steel pin, and the C injection was found to produce hardening [12,13]. Since analogous amorphizations of steels by P and C implantation were found to be less tribologically beneficial than the dual implantation of Ti and C [14,15], the latter treatment may also be superior for Ni.

Implantation of Ti and C may benefit micro-electromechanical systems (MEMS) constructed from electroformed Ni-based materials [16-18]. The performance and lifetime of such devices would be enhanced by hardening and reductions in friction and wear, and implantation accomplishes such reductions without the dimensional changes and debris formation that may accompany deposition of lubricious films.

In the present study, we explored the influence of Ti+C implantation on the elastic and plastic mechanical properties and the friction and wear characteristics of annealed bulk Ni, electroformed Ni, and $Ni_{80}Fe_{20}$, the latter two materials being used in MEMS. The Young's elastic modulus, yield strength, and hardness of the amorphous implanted layer were quantified through nanoindentation testing and finite-element modeling of the resultant deformation. Friction and wear were measured for a hard steel pin sliding without lubrication on treated and untreated surfaces.

## Elastic and plastic mechanical properties

Bulk Ni with a nominal purity of 99.99% was vacuum-annealed at 1273 K for 2 hours, resulting in observable grain relief with a typical grain size of several tenths of a millimeter.

Titanium was then implanted at 180 keV to a dose of $2\times10^{17}$ $cm^{-2}$, followed by the same dose of C at 45 keV. This produced the depth-dependent microstructure depicted in Fig. 1, as found by transmission electron microscopy (TEM). (See D. M. Follstaedt *et al.*, these proceedings, for a full discussion of composition and microstructure.) In layer II, which contained 16 at.% Ti and 22 at.% C as measured by ion-backscattering analysis, the matrix was fully amorphous. Layer I, with 18 at.% Ti and 16 at.% C, was mostly amorphous but contained inclusions of face-centered-cubic metal. Layer III, where the implanted concentrations of Ti and C were smaller but still several at.%, was fully crystalline with a high density of dislocations.

Mechanical properties were probed by nanoindentation [19] using a diamond tip with the Berkovich pyramidal shape. A slight rounding of the probe tip was quantified by calibration indentations of vitreous silica [20] and was included in the finite-element modeling to be discussed. Implanted and unimplanted Ni specimens were individually subjected to 10 indents on each of three grains, and plots of load versus depth are presented in Fig. 2. Included are data points from representative individual indents, together with dashed lines indicating the standard deviation for the 10 indents on the same grain when the deviation exceeds the size of the data points. The variation among grains is less than the indicated standard deviation.

To quantify the mechanical properties of the implanted region, finite-element modeling was used to simulate the indentation. The sample was approximated by several uniform layers, and parameters of the stress-strain curves within these layers were adjusted to produce agreement with experiment. (See J. A. Knapp *et al.*, these proceedings, for a description of the modeling and the extraction of parameters.) The adjusted quantities were Young's elastic modulus, E, and the yield strength at 0.2% elongation, Y; the work hardening rate of the crystalline regions was taken from the published stress-strain curve of polycrystalline Ni [21], while the work hardening rate of the amorphous zone was equated to zero in view of the absence of mobile dislocations. The implanted region was assumed to have zero stress before indentation, an approximation that calculations indicate could inflate the deduced strength by about 10% if initial compressive stress approached the yield strength. To facilitate comparisons of strength in the technologically important regime of large deformations, we defined an intrinsic hardness, $H_I$, as the asymptotic

ratio of indentation load to projected contact area for an imaginary, uniform substrate having the same stress-strain curve as the actual material at the depth of interest. This quantity was evaluated from the fitted stress-strain curve by finite-element modeling. For a uniform, semi-infinite specimen, $H_I$ reduces to conventional hardness.

Results of the above fitting procedure for unimplanted and implanted annealed bulk Ni are given by the solid curves in Fig. 2. In the case of the unimplanted specimen, the data are consistent with a single elastic modulus of 220 GPa, in good agreement with the published value of 207 GPa [22]. The apparent yield strength varies with depth, however, as shown by the dashed line in Fig. 3: the Y employed in the calculations decays approximately exponentially from a high of 0.65 GPa in the near-surface region to an asymptotic value of 0.15 GPa at large depths, which is within the range of literature values [22]. Previous workers have also reported an upward excursion in indentation hardness in the near-surface of unimplanted Ni [13], and we have found a similar phenomenon in well annealed unimplanted Al. We have not seen this effect in fine-grained, ion-implanted, or otherwise highly refined microstructures, however, including the electroformed Ni and $Ni_{80}Fe_{20}$ materials to be discussed hereinafter. Hence, the cause may be sluggishness in the initial formation of dislocations in the absence of lattice imperfections.

In modeling the implanted annealed bulk Ni, we allowed Y and E to vary independently for the implantation-affected layers I, II, and III depicted in Fig. 1, but the properties of the underlying material were required to conform to those deduced for the unimplanted specimen. The resulting depth-dependent Y is given by the solid line in Fig. 3. Particularly noteworthy is the large yield strength of the amorphous layer II, 4.7 GPa. Implantation produces a smaller but significant increase in E to 440 GPa.

The extraction of the rather detailed depth dependence of Y in Fig. 3 for the implanted specimen warrants further justification. The localization of the hardening within the near-surface region is evident simply from the general shape of the indentation data in Fig. 2, where an initially parabolic rise in load with depth gives way to an inflection and reduced slope at greater penetrations. The resolution of differences in Y among layers I-III is a more subtle matter, however. The extent to which this is feasible is illustrated in Fig. 4, where the difference between

the calculated and measured loads is plotted for two fitted simulations. The simulation represented by the dashed line is the one discussed above, where the strengths of layers I, II, and III were independently varied. In the simulation represented by the solid line, the implanted region was approximated as a single, uniform layer extending from the surface to 180 nm. The latter calculation is seen to depart systematically from the experimental data, by an amount comparable to the standard deviation, whereas the use of three independent layers results in significantly better agreement. The peak yield strength derived from the single-layer analysis is 4.1 GPa, not greatly different from the 4.7 GPa obtained using three layers.

We carried out similar nanoindentation studies of the effects of Ti+C implantation on the mechanical properties of electroformed Ni and $Ni_{80}Fe_{20}$. Test specimens of 0.15-mm thickness were synthesized in conjunction with micromachine components by electroplating from a sulfamate bath at 50°C using a current density of 50 $mA/cm^2$. Transmission electron microscopy revealed very small grain sizes in the range 30-600 nm, which gives rise to a hardness substantially greater than that of annealed bulk Ni. The fully amorphous region produced by implantation was observed by TEM to extend to the surface in the electroformed Ni, and there were only isolated near-surface inclusions of crystalline metal in the $Ni_{80}Fe_{20}$ alloy, in contrast to the microstructure of annealed bulk Ni depicted in Fig. 1. This difference may reflect the influence of defects or impurities initially present in the near-surface region of the electroformed materials. The finite-element modeling of the electroformed materials assumed a single, uniform implantation-affected layer extending from the surface to 160 nm. Indentation data from the unimplanted specimens showed no evidence of a variation of Y with depth.

The deduced mechanical properties for all of the investigated materials are summarized in Fig. 5. The values listed for unimplanted materials reflect bulk properties, whereas the values for implanted specimens represent the fully amorphous layer. Included for comparison are properties of two high-strength bulk materials, rapidly solidified amorphous $Fe_{40}Ni_{40}B_{20}$ [23] and martensitic Type 440C bearing steel [8,24,25].

**Tribology**

Unlubricated friction and wear were examined for the unimplanted and implanted materials in contact with a sliding steel pin. The pin was of Type 440 C bearing steel, and the tip was spherical with a radius of 1.6 mm. In the case of annealed bulk Ni, friction was measured on rotating discs of the unimplanted and implanted material in dry nitrogen ambient. The applied load was 9 g, corresponding to a peak Hertzian contact stress of 43 MPa. Before tribological testing of the implanted specimen, an additional implant of $3\times10^{16}$ C/cm$^2$ at 20 keV removed the residual crystalline inclusions in the near surface region. The measured friction coefficients are shown in Fig. 6. The trace for unimplanted material exhibits pronounced oscillations, reflecting destructive adhesion-and-fracture wear. In contrast, a more stable frictional force is observed for the implanted material before breakthrough of the hardened layer above 100 cycles, consistent with replacement of the destructive wear mode by mild abrasive wear. The average friction coefficient is also reduced by the implantation treatment.

Wear tracks for unimplanted and implanted annealed bulk Ni were profiled after cyclical linear sliding of the steel pin in laboratory air with an applied load of 10 g. Representative topographies, obtained by scanning interferometry, are shown in Fig. 7. The destructive adhesion-and-fracture wear produces a jagged track on the unimplanted specimen, where after 67 cycles the maximum wear depth is 1.82 μm. The mild abrasive wear on the implanted specimen gives rise to a much smoother wear track, and the maximum wear depth is only 0.28 μm after 100 cycles.

We also examined the friction characteristics of unimplanted and implanted electroformed Ni, using a cyclical linear pin motion with an applied load of 10 g in laboratory air, and the results are shown in Fig. 8. The implantation treatment again causes a change of wear mode from adhesion-and-fraction to mild abrasion. The friction coefficient is reduced further than in Fig. 6, reaching a value of about 0.3.

**Discussion**

The yield strengths of about 5 GPa and intrinsic hardnesses near 14 GPa deduced for the implanted amorphous Ni-Ti-C layer are exceptionally large for alloys based on Ni and Fe. This

is seen in Fig. 5, which provides comparisons with two of the hardest types of Ni-Fe materials previously available, martensitic steels and metalloid-stabilized amorphous alloys. The yield strength and elastic modulus of the implanted amorphous phase are about twice those of the latter materials, and the hardness is also substantially greater. We hypothesize that the exceptional strength of the implanted layer arises from the combination of two effects. First, in an amorphous alloy, plastic flow by dislocations glide is absent. Consequently, for Ni-Fe amorphous alloys not containing Ti and C, yielding is typically found at 2-3 GPa, with indentation hardnesses of ~7-11 GPa [23]. The second hypothesized contribution to high strength is binding reactions between Ti and C atoms within the matrix. Evidence for this effect comes from studies of rapidly quenched amorphous alloys containing C; for example, introducing Ti so as to go from amorphous $Fe_{70}Mo_{12}C_{18}$ to $Fe_{68}Ti_2Mo_{12}C_{18}$, increased the hardness by about 1 GPa [26]. While the detailed dependence of this effect on Ti concentration was not reported, we assume as a first approximation that it is linear. Then, for the present case, where the Ti concentration is 16 at.%, a hardness increment of ~8 GPa is estimated. Summing the two hypothesized contributions gives (~7 to 11 GPa) + (~ 8GPa) = (~15 to 19 GPa), in semiquantitative agreement with the hardness extracted from our experiments.

We hypothesize that the reductions in friction and wear caused by implantation of Ti and C are due largely to the hardening of the near-surface layer. The resultant reduction of deformation during sliding contact reduces substantially the area over which adhesion can occur. Moreover, the greatly strengthened surface region should be more resistant to the kind of fracture evidenced by the irregular morphology seen in Fig. 7(a). It is also possible that the altered composition of the implanted alloy gives rise to differences in surface oxide and surface chemistry that may influence the tribology.

Based on the above findings, Ti+C implantation appears promising for application to MEMS.

**Acknowledgments**

The implantations were carried out by G. A. Petersen, and M. P. Moran prepared specimens for TEM. This work was supported by the U. S. Dept. of Energy, Office of Basic Energy Sciences, under Contract DE-AC04-94AL85000.

**References**


1. D. M. Follstaedt, J. A. Knapp, and S. T. Picraux, Appl. Phys. Lett. 37 (1980) 330.

2. J. A. Knapp, D. M. Follstaedt, and B. L. Doyle, Nucl. Instrum. Methods B 7-8 (1985) 38.

3. A. W. Mullendore, L. E. Pope, A. K. Hays, G. C. Nelson, C. R. Hills, and B. G. LeFevre, Thin Solid Films 186 (1990) 215.

4. I. L. Singer, C. A. Carosella, and J. R. Reed, Nucl. Instrum. Methods 182-183 (1981) 923.

5. D. M. Follstaedt, F. G. Yost, and L. E. Pope, Mat. Res. Soc. Symp. Proc. 27 (1984) 655.

6. D. M. Follstaedt, J. A. Knapp, and L. E. Pope, Nucl. Instrum. Methods B 42 (1989) 205.

7. C. A. Carosella, I. L. Singer, R. C. Bowers, and C. R. Gossett, in Ion Implantation Metallurgy, edited by C. M. Preece and J. K. Hirvonen, TMS-AIME, Warrendale, Pennsylvania, 1980, pp. 103-115.

8. L. E. Pope, F. G. Yost, D. M. Follstaedt, J. A. Knapp, and S. T. Picraux, in Wear of Materials, edited by K. C. Ludema, ASME, New York, 1983, pp. 280-287.

9. D. M. Follstaedt, J. A. Knapp, L. E. Pope, F. G. Yost, and S. T. Picraux, Appl. Phys. Lett. 45 (1984) 529.

10. D. M. Follstaedt, Nucl. Instrum. Methods B 10-11 (1985) 549.

11. W. C. Oliver, R. Hutchings, J. B. Pethica, I. L. Singer, and G. K. Hubler, Mat. Res. Soc. Symp. Proc. 27 (1984) 603.

12. J. Takadoum, J. C. Pivin, J. Chaumont, and C. Roque-Carmes, J. Mater. Sci. 20 (1985) 1480.

13. M. Nastasi, J.-P. Hirvonen, T. R. Jervis, G. M. Pharr, and W. C. Oliver, J. Mater. Res. 3 (1988) 226.

14. L. E. Pope, S. T. Picraux, D. M. Follstaedt, J. A. Knapp, and F. G. Yost, J. Mater. for Energy Sys. 7 (1985) 27.

15. D. M. Follstaedt, J. A. Knapp, and L. E. Pope, J. Appl. Phys. 66 (1989) 2743.

16. E. W. Becker, W. Ehrfeld, P. Hagmann, A. Maner, and D. Münchmeyer, Microelectron. Eng. 4 (1986) 35.

17. H. Guckel, K. J. Skrobis, J. Klein, and T. R. Christenson, J. Vac. Sci. Technol. A 12 (1994) 2559.

18. T. R. Christenson and H. Guckel, SPIE Proc. 2639 (1995) 134.

19. Indentation testing was carried out by B. N. Lucas at Nano Instruments, Inc., in Oak Ridge, Tennessee.

20. W. C. Oliver and G. M. Pharr, J. Mater. Res. 7 (1992) 1564.

21. Atlas of Stress-Strain Curves, edited by H. E. Boyer, ASM, Metals Park, Ohio, 1987, p. 551.

22. Metals Handbook, vol. 2 (ASM, 1990) pp. 437, 1143.

23. J. Niebuhr, R. Gerber, A. Schaller, and H.-W. Müller, Physical Data of Amorphous Metals, Part B: Data Tables, Fachinformationszentrum Karlsruhe, Freiburg, Germany, 1991, p. 239.

24. L. E. Pope, F. G. Yost, D. M. Follstaedt, S. T. Picraux, and J. A. Knapp, Mat. Res. Soc. Symp. Proc. 27 (1984) 661.

25. Aerospace Structural Metals Handbook, edited by W. F. Brown, Jr., H. Mindlin, and C. Y. Ho, Purdue Research Foundation, West Lafayette, Indiana, 1996, pp. 1405-1 to 1505-5.

26. A Inoue, T. Iwadachi, T. Minemura, and T. Masumoto, Trans. Jap. Inst. Metals 22 (1981) 197.

**Figure captions**

1. Depth-dependent microstructure of annealed bulk Ni implanted with $2\times10^{17}$ Ti/cm$^2$ at 180 keV and $2\times10^{17}$ C/cm$^2$ at 45 keV.
2. Nanoindentation data and fitted finite-element simulations for annealed bulk Ni with and without implantation of Ti+C.
3. Depth-dependent yield strengths employed in the finite-element modeling for implanted and unimplanted annealed bulk Ni.
4 Differences between experimental indentation data and fitted simulations resulting from the use of one or three layers to model the implanted region.
5. Mechanical properties derived from indentation testing, compared with the properties of two high-strength bulk materials.
6. Friction coefficients for unimplanted and implanted annealed bulk Ni, as measured using a rotating disc in dry nitrogen.
7 Wear-track topographies for (a) unimplanted annealed bulk Ni after 67 cycles and (b) implanted material after 100 cycles, after testing with a cyclical linear pin motion in laboratory air.
8. Friction coefficients for unimplanted and implanted electroformed Ni, as measured using a cyclical linear pin motion in laboratory air.

| I | II | III | IV |
|---|---|---|---|
| Amor. + Cryst. | Amorphous Ni(Ti,C) | Crystalline dislocated Ni(Ti,C) | Unaffected Ni |
| 30 nm | ← 50 nm → | ← 100 nm → | |

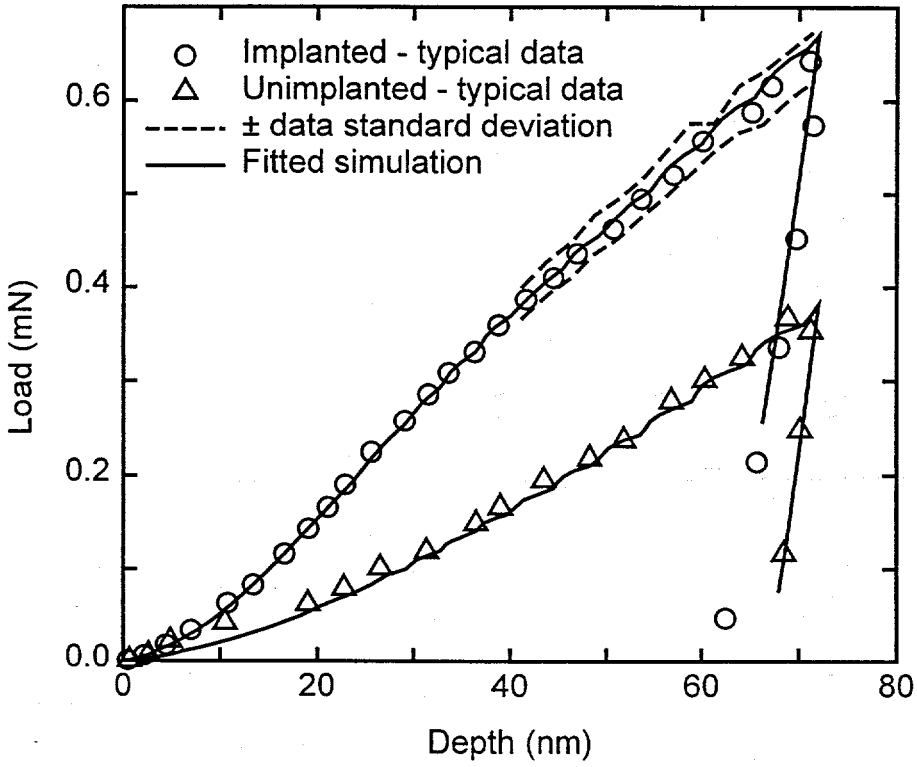

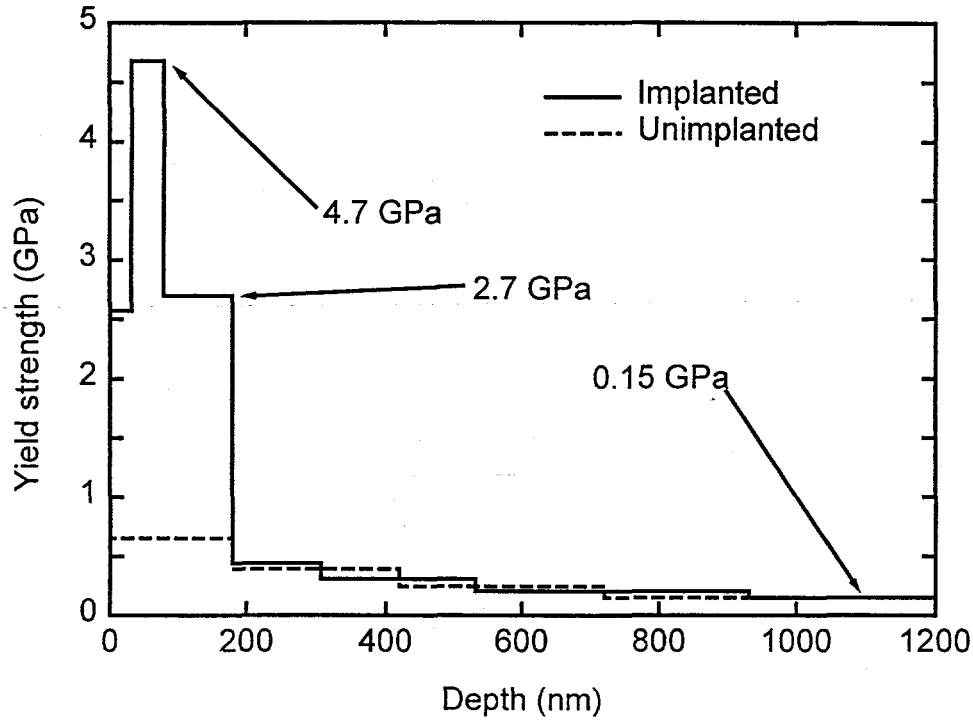
Implanted
Unimplanted
4.7 GPa
2.7 GPa
0.15 GPa
Yield strength (GPa)
Depth (nm)
0
1
2
3
4
5
0
200
400
600
800
1000
1200

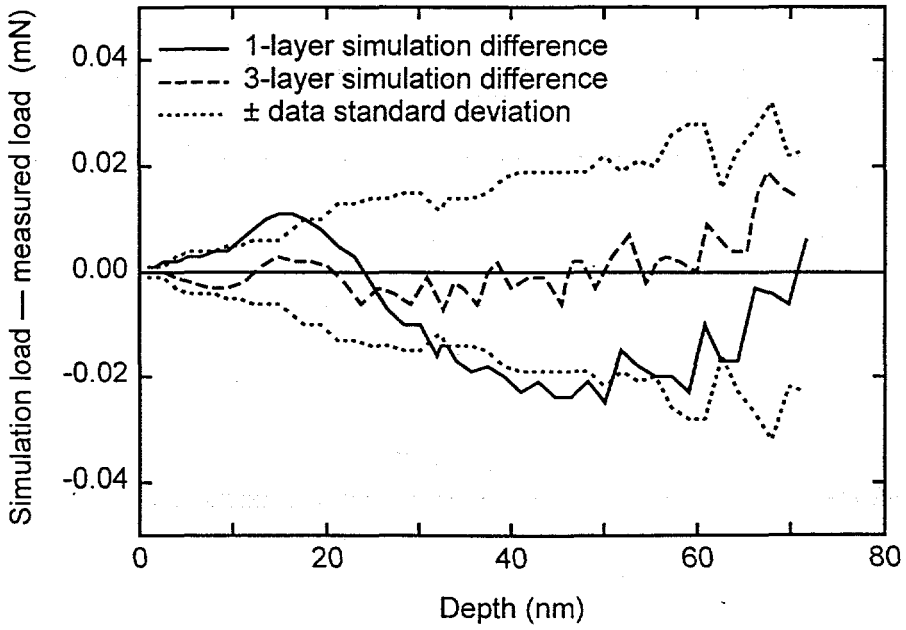
1-layer simulation difference
3-layer simulation difference
± data standard deviation
Simulation load — measured load (mN)
Depth (nm)
0.04
0.02
0.00
-0.02
-0.04
0
20
40
60
80

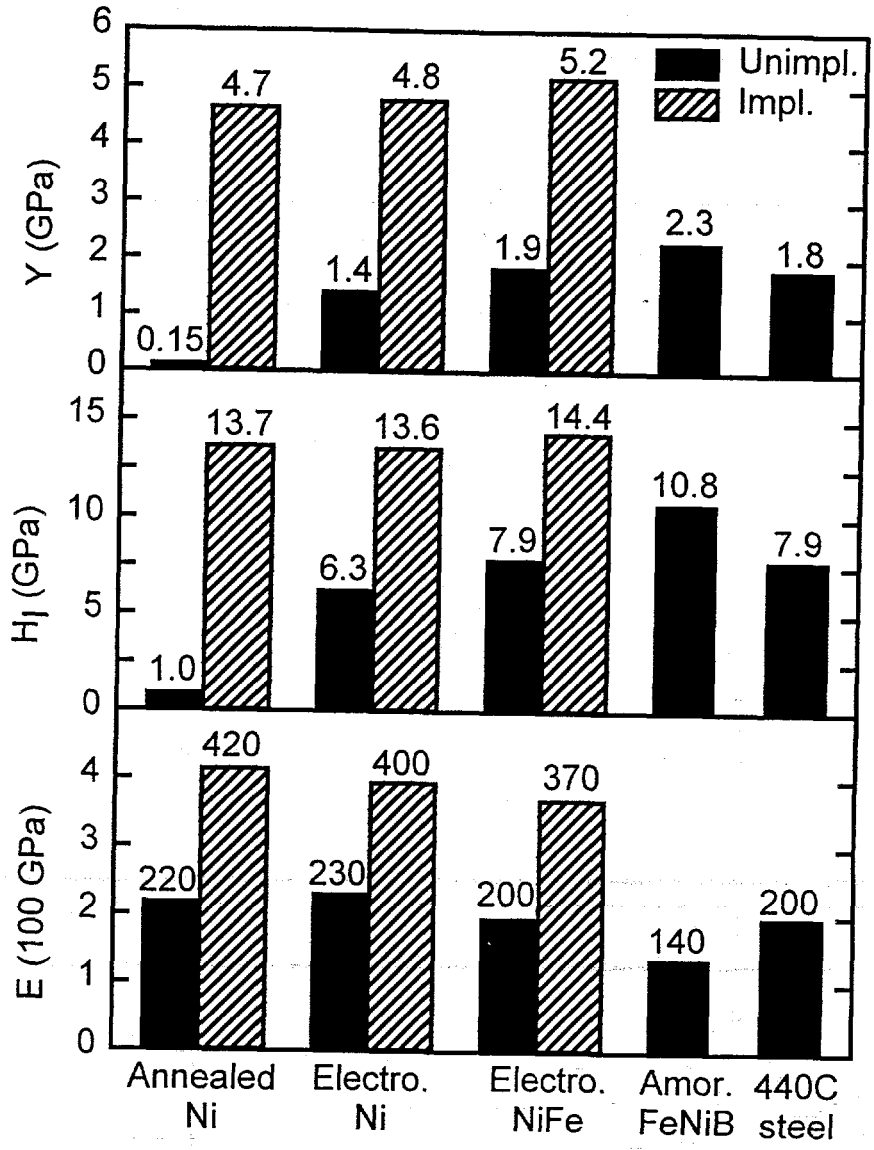
Y (GPa)
H_I (GPa)
E (100 GPa)
Unimpl.
Impl.
0.15
4.7
1.4
4.8
1.9
5.2
2.3
1.8
1.0
13.7
6.3
13.6
7.9
14.4
10.8
7.9
220
420
230
400
200
370
140
200
Annealed Ni
Electro. Ni
Electro. NiFe
Amor. FeNiB
440C steel

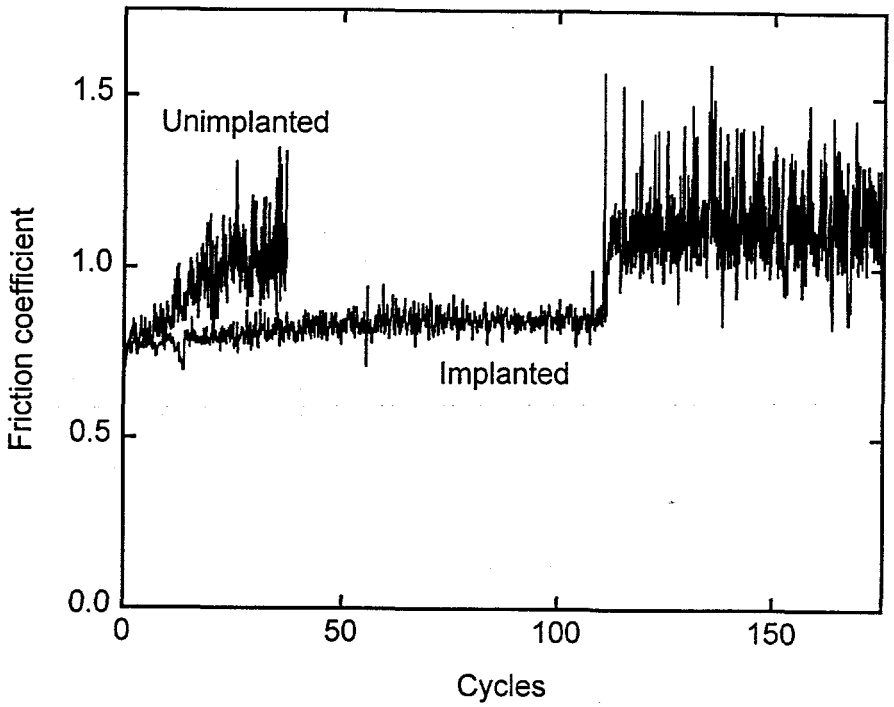
Friction coefficient
1.5
1.0
0.5
0.0
Unimplanted
Implanted
0
50
100
150
Cycles

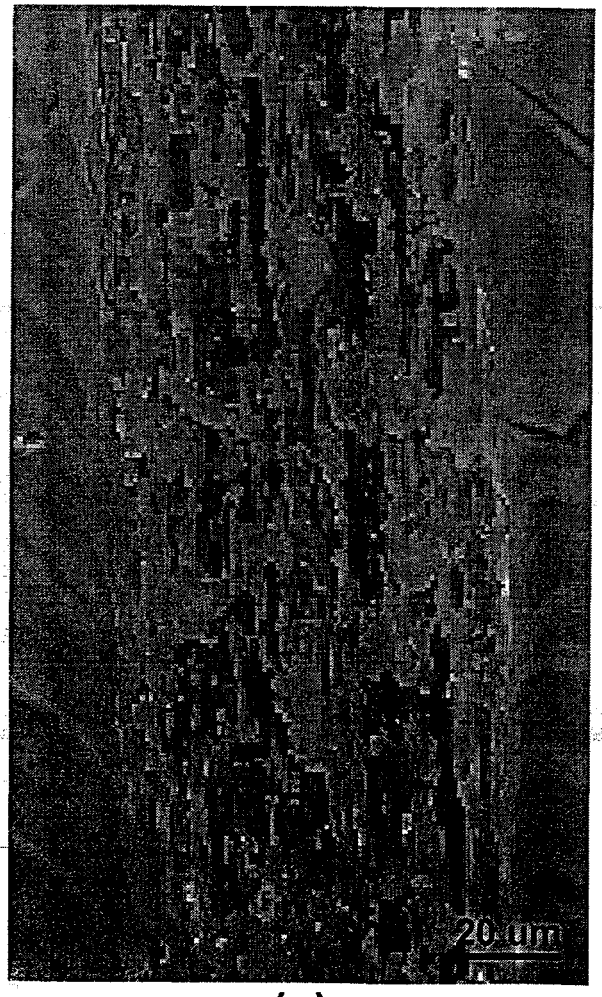
20 μm

(a)

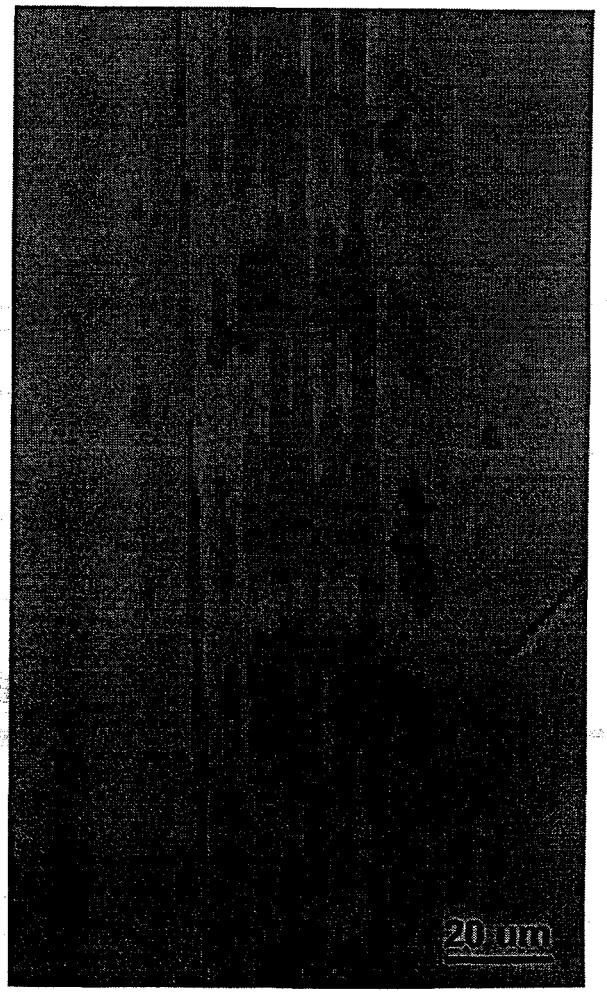
20 μm

(b)

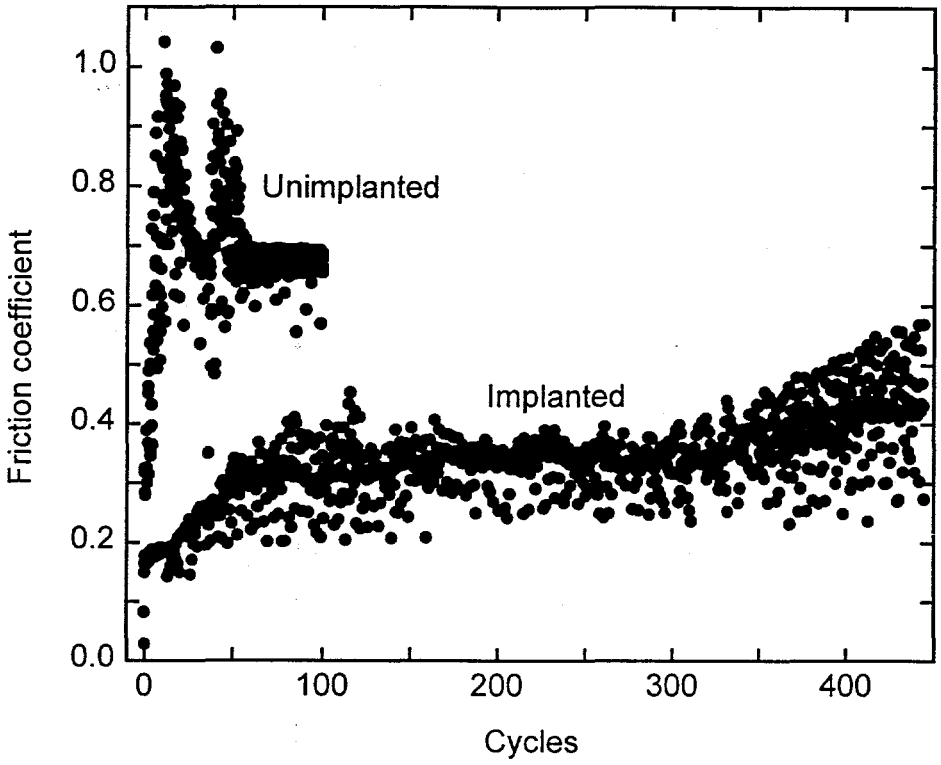
Friction coefficient
1.0
0.8
0.6
0.4
0.2
0.0
Unimplanted
Implanted
0
100
200
300
400
Cycles